

UC Santa Barbara

UC Santa Barbara Previously Published Works

Title

Seismic Envelope-Based Detection and Location of Ground-Coupled Airwaves from Volcanoes in Alaska
Seismic Envelope-Based Detection and Location of Ground-Coupled Airwaves from Volcanoes in Alaska

Permalink

<https://escholarship.org/uc/item/91q1s7hc>

Journal

Bulletin of the Seismological Society of America, 106(3)

ISSN

0037-1106

Authors

Fee, David
Haney, Matt
Matoza, Robin
et al.

Publication Date

2016-06-01

DOI

10.1785/0120150244

Copyright Information

This work is made available under the terms of a Creative Commons Attribution-NonCommercial-NoDerivatives License, available at <https://creativecommons.org/licenses/by-nc-nd/4.0/>

Peer reviewed

Seismic Envelope-Based Detection and Location of Ground-Coupled Airwaves from Volcanoes in Alaska

by David Fee,* Matt Haney, Robin Matoza, Curt Szuberla, John Lyons, and Chris Waythomas

Abstract Volcanic explosions and other infrasonic sources frequently produce acoustic waves that are recorded by seismometers. Here we explore multiple techniques to detect, locate, and characterize ground-coupled airwaves (GCA) on volcano seismic networks in Alaska. GCA waveforms are typically incoherent between stations, thus we use envelope-based techniques in our analyses. For distant sources and planar waves, we use f - k beamforming to estimate back azimuth and trace velocity parameters. For spherical waves originating within the network, we use two related time difference of arrival (TDOA) methods to detect and localize the source. We investigate a modified envelope function to enhance the signal-to-noise ratio and emphasize both high energies and energy contrasts within a spectrogram. We apply these methods to recent eruptions from Cleveland, Veniaminof, and Pavlof Volcanoes, Alaska. Array processing of GCA from Cleveland Volcano on 4 May 2013 produces robust detection and wave characterization. Our modified envelopes substantially improve the short-term average/long-term average ratios, enhancing explosion detection. We detect GCA within both the Veniaminof and Pavlof networks from the 2007 and 2013–2014 activity, indicating repeated volcanic explosions. Event clustering and forward modeling suggests that high-resolution localization is possible for GCA on typical volcano seismic networks. These results indicate that GCA can be used to help detect, locate, characterize, and monitor volcanic eruptions, particularly in difficult-to-monitor regions. We have implemented these GCA detection algorithms into our operational volcano-monitoring algorithms at the Alaska Volcano Observatory.

Introduction

Low-frequency acoustic waves (infrasound) are often recorded by seismometers, particularly near volcanoes and in regions where energetic acoustic signals are common. These signals have been considered as representing an acoustic wave impinging on the Earth's surface and coupling into the ground in the form of a Rayleigh or Stoneley wave (Ben-Menahem and Singh, 1981; Edwards *et al.*, 2007; Ichihara *et al.*, 2012). Often these signals are ignored or considered noise and not identified in seismic catalogs (Cochran and Shearer, 2006). Although they do not make for ideal acoustic recordings, these ground-coupled airwaves (GCA) have been used to detect and characterize volcanic explosions (Johnson and Malone, 2007; De Angelis *et al.*, 2012), meteors (Edwards *et al.*, 2007), and large acoustic signals in general (Cochran and Shearer, 2006; Walker *et al.*, 2011), as well as to infer atmospheric structure (Hedlin *et al.*, 2012). Recent work has used cross correlation and coherence techniques to identify infrasound signals on colocated seismic and acoustic

sensors (Ichihara *et al.*, 2012) and to differentiate between seismic and acoustic waves (Matoza and Fee, 2014).

Infrasonic waves are being increasingly used to detect and characterize volcanic eruptions, both on a local and global scale (Fee and Matoza, 2013). Monitoring volcanic eruptions is challenging and can be expensive, particularly in remote locations such as Alaska. Clouds and image delays can inhibit satellite remote sensing, and ground-based systems (such as seismic systems) are expensive and difficult to maintain. The resulting data can be ambiguous concerning surficial volcanic activity. Infrasound can provide valuable quantitative information about eruption dynamics (such as volume flux) that are otherwise challenging to obtain, particularly in real time. Infrasound networks, however, are still relatively sparse when compared with their seismic counterparts. Utilizing GCA on seismometers thus supplements existing infrasound networks and provides additional information on the eruptions that would otherwise not be available. Ideally, we would have dense seismic and acoustic networks to capture unperturbed, complementary waveforms; however, because this is not feasible in many locations, we use any available data.

*Also at Wilson Alaska Technical Center, Geophysical Institute, University of Alaska Fairbanks, 903 Koyukuk Drive, Fairbanks, Alaska 99775.

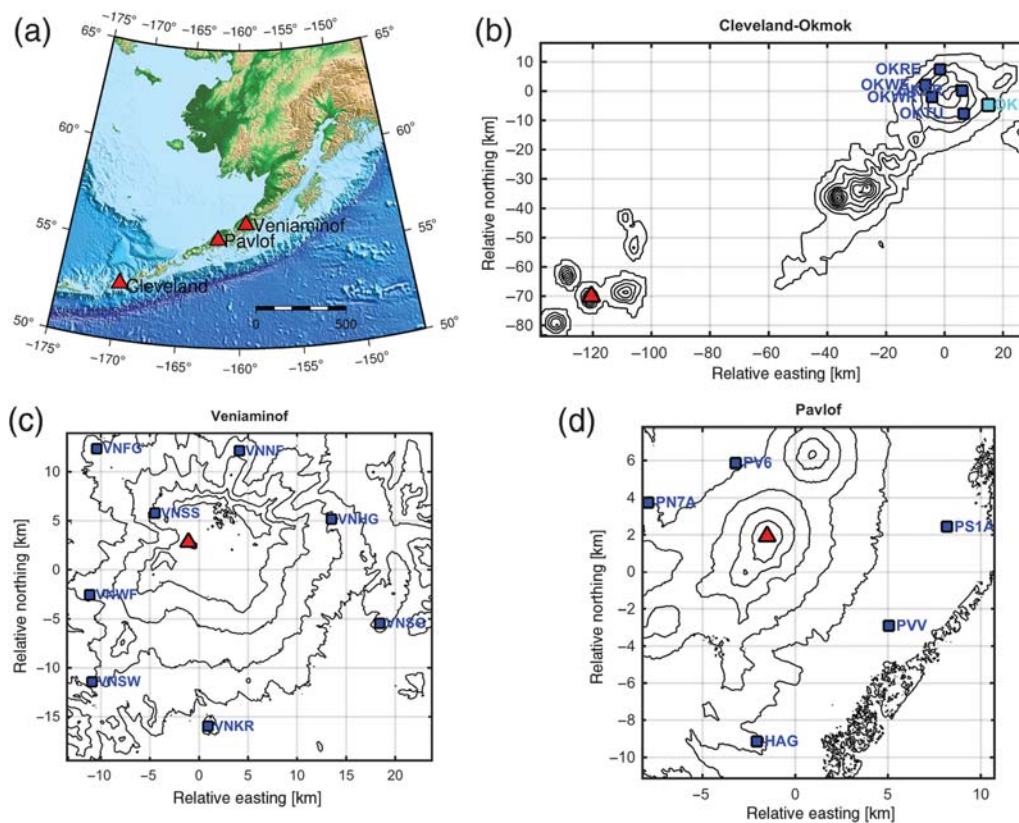


Figure 1. Map and network layouts. (a) Alaska and the three studied volcanoes. (b) Cleveland Volcano (red triangle) in relation to the Okmok seismic network $\sim 130\text{--}150$ km distant. (c) Mt. Veniaminof and associated seismic network, consisting of 10 stations spread over an $\sim 30 \times 30$ km² region. (d) Pavlof Volcano and seismic network of five stations over $\sim 16 \times 15$ km². Contours in (b–d) are determined from ASTER and ETOPO datasets and are shown at 200, 400, and 400 m, respectively.

Detection and location of GCA are complicated by variable coupling and a lack of waveform coherence between stations (De Angelis *et al.*, 2012; Matoza and Fee, 2014). In this article, we explore (1) the use of GCA to detect, locate, and characterize volcanic explosions in Alaska; (2) the methods for GCA detection and localization when standard waveform cross-correlation fails; and (3) techniques to infer information on the volcanic explosions themselves and to show how they can be useful for volcano monitoring. In particular, we focus on envelope-based techniques and consider scenarios in which the explosion occurs both within the network (modeled as a curved wavefront radiating outward) and outside the network (modeled as a plane wave traversing the network).

Data

We utilize seismic data from networks installed and operated by the Alaska Volcano Observatory (AVO) near volcanoes with explosive activity between 2007 and 2015. These networks are located in remote regions of Alaska and the Aleutian Islands (Fig. 1) (Dixon *et al.*, 2015). They represent a mix of short-period and broadband seismometers in various configurations and environments. Short-period instruments are sampled at 100 Hz and broadbands at 50 Hz.

The following paragraphs detail the networks selected and provide some information on the eruptions studied.

Cleveland Volcano is a regularly active and very remote volcano in the central Aleutian Islands (Fig. 1). Prior to 2014, no local monitoring network existed, and the volcano was primarily monitored using satellite data and remote seismic and infrasound networks. We refer to De Angelis *et al.* (2012) for more information on recent eruptions and geophysical observations from Cleveland Volcano. For our analysis of Cleveland Volcano, we use data from the seismic network on Okmok Volcano, located ~ 140 km to the northeast on Umnak Island (Fig. 1b). This network comprises eight short-period and four broadband sensors spread about Umnak Island. We evaluated an eruption from Cleveland Volcano that occurred in May 2013 and was recorded well by the five operational short-period stations of the Okmok network. No data were received from the broadband stations. This explosion is representative of activity at the volcano during this period, which consisted of days to weeks of quiescence punctuated by short-duration explosive events that produced small amounts of tephra that fell primarily on the upper flanks of the volcano.

Mount Veniaminof Volcano is a large (> 300 km³), active volcano located on the Alaska Peninsula (Fig. 1). It is

Table 1
Summary of Principal Methods Used in this Study

Method	Description	Dataset
Modified spectrogram*	Multitaper spectrogram scalar function to emphasize high energy and high-energy contrast	All
f - k beamforming†	Slowness-based plane-wave characterization	Cleveland Volcano 2013, Okmok seismic network
$srcLoc$ ‡	Time difference of arrival (TDOA) localization using analytical least-squares inversion for spherical acoustic waves	Pavlof Volcano 2007, 2013; Veniaminof Volcano 2013
SPDD§	TDOA localization using station-pair differential travel times	Pavlof Volcano 2007, 2013; Veniaminof Volcano 2013

*Withers *et al.* (1998) and Gibbons *et al.* (2008).

†For example Johnson and Dudgeon (1992).

‡Szuberla *et al.* (2009) and Rowell *et al.* (2014).

§Zhang *et al.* (2010) and Haney (2010). SPDD, station-pair double difference.

composed of a broad edifice with an 8×11 km² ice-filled summit caldera (Miller *et al.*, 1998). Frequent small-scale eruptions have occurred from an intracaldera cone over the past 30 years. The most recent eruption occurred between 13 June and approximately 20 September 2013 and consisted of mainly low-level explosions and sustained seismic tremor. Lava flows erupted in 2013 and flowed off the intracaldera cone onto the surrounding ice field, but they did not produce significant melt (Schneider *et al.*, 2013; Dixon *et al.*, 2015). Veniaminof is monitored by AVO using an eight-station seismic network (Fig. 1c), satellite data, limited visual observations from the nearby community of Perryville, and remote infrasound arrays. We search for GCA on all eight seismic stations of the Veniaminof network.

Pavlof Volcano is a frequently active volcano located on the lower Alaska Peninsula (Fig. 1). We focus on two recent eruptions: August–September 2007 and May–October 2013. These eruptions both consisted of sustained lava fountaining and intermittent, short-duration explosions. Ash plumes were emitted up to 8 km above sea level, and extended up to 500 km from the volcano. Accumulation of spatter occasionally led to small hot granular avalanches and lahars (Waythomas *et al.*, 2008, 2014; Haney *et al.*, 2009; Dixon *et al.*, 2015). AVO operates a five-station short-period seismic network around Pavlof (Fig. 1d) and uses this and satellite data, limited visual observations, and remote infrasound arrays to monitor the volcano. Two seismic stations on the north side of the volcano (PV6 and PN7A) were not operating in 2013. A single infrasound sensor located at station PN7A was installed during the eruption in 2007 and was not functioning during the 2013 eruption. It is important to note that the active volcanic cone is located within the seismic networks at both Veniaminof and Pavlof, whereas the Okmok network is over 130 km from Cleveland Volcano.

Methods

We experiment with multiple-event detection and localization techniques for GCA on the aforementioned volcano seismic networks. Localization is divided into two regimes based on the relative location of the source and network (Szuberla *et al.*, 2006): in-network and out-of-network. The

out-of-network case applies to a source at great distance from the network, where the acoustic source can be considered to be in the far field and the incident wave is planar as it propagates across the network. The in-network case applies to sources within the seismic network where the acoustic wave is in the near field, radiating outward as a curved wavefront across the network. Table 1 provides a summary of the principal detection and location methods used.

Waveforms are first filtered using a four-pole, zero-phase, Butterworth filter. The amplitude envelope is calculated from the absolute value of the analytic signal of the waveform, also termed the analytic envelope. Envelopes are detrended and smoothed with a fast Fourier transform-based 1-s-long convolutional filter to remove long-term bias and filter out short-term noise. After the envelope is calculated for each waveform, short-term average/long-term average (STA/LTA) is applied with 1 s STA and 10 s LTA windows. Only vertical components are used.

Modified Spectrogram

In addition to taking the envelope of a filtered waveform, we experiment with modifying the envelope function to improve the detection and location of acoustic arrivals following the methods of Withers *et al.* (1998) and particularly Gibbons *et al.* (2008). They modified the envelope function to enhance regions of a time series that show both high energy and a high-energy contrast between spectrogram windows. This “incoherent array processing” is particularly effective in increasing the signal-to-noise ratio (SNR) of signals within the envelopes and aiding array processing when cross correlation of waveforms fails. This method has three major steps and is illustrated on GCA in seismic data in Figure 2. First, a spectrogram $A(f, t)$ is constructed from the unfiltered data using the multitaper method of Thomson (1982) (Fig. 2b). A multitaper spectrogram permits relatively high-resolution, stable spectral estimates of short data segments at the cost of being computationally expensive. We use a window length of 4 s with successive overlapping windows. A modified spectrogram $S(f, t)$ is then computed to highlight changes in spectrogram energy as a function of time (Gibbons *et al.*, 2008):

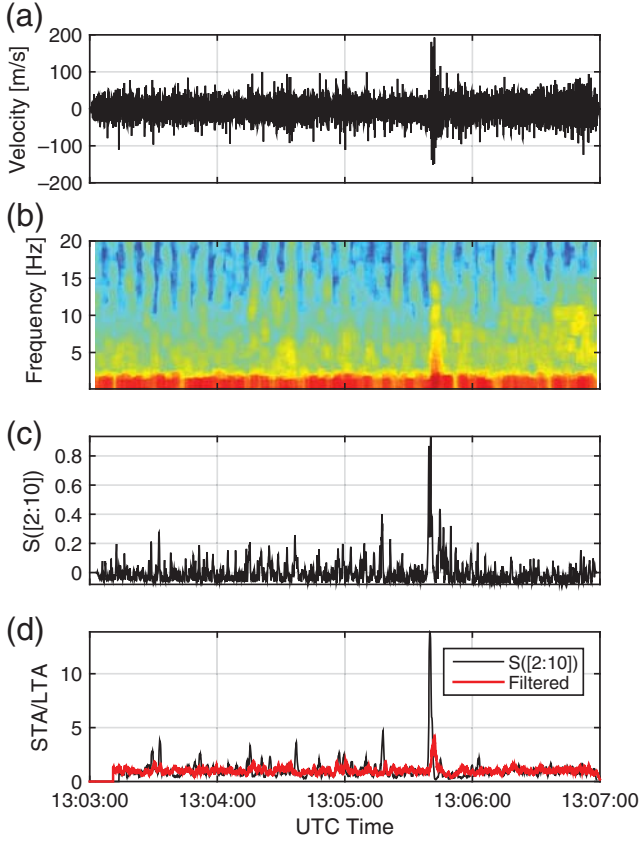


Figure 2. Modified spectrogram envelope technique based on Gibbons *et al.* (2008). (a) 2–10 Hz filtered waveform for an explosion from Cleveland Volcano. (b) Multitaper spectrogram between 0.1 and 20 Hz. (c) Scalar function derived from the multitaper spectrogram between 2 and 10 Hz. (d) Comparison of short-term average/long-term average (STA/LTA) ratios for the filtered data in (a) (red) and scalar function from (c) (black).

$$S(f, t) = (\log_{10}[A(f)_{t+}] - \log_{10}[A(f)_{t-}]) \log_{10}[A(f)_{t+}], \quad (1)$$

in which the current value of the spectrogram time window $[A(f, t)_{t+}]$, is multiplied by the difference between the current and preceding $[A(f, t)_{t-}]$ values, then multiplied by itself. Last, a scalar function (or modified envelope) is constructed over a frequency band of interest (Gibbons *et al.*, 2008):

$$\bar{S}([f_1 : f_2], t) = \exp \left[\frac{1}{N_f} \sum_{f=f_1}^{f_2} S(f, t) \right], \quad (2)$$

in which N_f is the number of discrete frequencies between f_1 and f_2 (Fig. 2c). The exponential has the effect of deemphasizing negative changes in energy contrast between two spectrogram windows. The reader is referred to Gibbons *et al.* (2008) and Gibbons (2014) for detailed discussion on this technique. Standard STA/LTA analysis can then be applied to look for arrivals of interest.

Out-of-Network Localization

For the out-of-network case, we are limited to slowness vector estimation rather than localization because the wave crossing the network is assumed to be roughly planar. We employ a commonly used array processing technique for slowness vector estimation: f - k beamforming of the envelopes is used to determine the trace velocity (velocity of the wave across the network) as well as the back azimuth (bearing from the north) to the source. Least-squares estimation produces similar results to f - k .

In-Network Localization

In-network localization is more complex, and we explore the effectiveness of two different, but related, methods. We apply two time difference of arrival (TDOA) methods to determine the lateral (2D) geographic location of the source. TDOA methods invert for source location parameters using differential travel times between station pairs. Differential travel times are determined for both TDOA methods from cross correlation of envelopes due to the aforementioned lack of waveform coherency of the GCA used in this study. The first TDOA method is termed *srcLoc*. It has been used extensively for near-source localization of infrasound data and has been found to provide substantially more accurate source localization than back-azimuth-based techniques (Szuberla *et al.*, 2009). The *srcLoc* technique consists of a two-stage localization process for best-fitting time difference of arrivals: least-squares inversion for source location followed by a numerical optimization process. The least-squares inversion is solved analytically for the wavespeed, source location, and absolute arrival times by finding the best-fitting 3D, hyperbolic space–time cone. This space–time cone can be visualized as sound radiating out spherically in time from a 2D source location. The inverse solution is then used as a seed into a Nelder–Mead optimization. A minimum of four sensors are required for this technique. Compared to traditional earthquake location methods that rely on grid search or optimization, *srcLoc* solves for the solution analytically. In addition, the second stage avoids the inversion being caught in a local minima. See Szuberla *et al.* (2009), Szuberla and Arnoult (2011), and Rowell *et al.* (2014) for additional details on *srcLoc*.

The second in-network TDOA localization method is station-pair double difference (SPDD). Rather than use event-pair differential travel times, as is common in earthquake location (e.g., Waldhauser and Ellsworth, 2000), SPDD relies on differential arrival times between station pairs from common events (Obara, 2002; Haney, 2010; Zhang *et al.*, 2010). Following the nomenclature of Zhang *et al.* (2010), for a single event we can estimate the travel-time residual for two stations i and j as

$$r_i = \sum_{m=1}^2 \frac{\partial T_i}{\partial x_m} \Delta x_m + \Delta \tau \quad (3)$$

and

$$r_j = \sum_{m=1}^2 \frac{\partial T_j}{\partial x_m} \Delta x_m + \Delta \tau, \quad (4)$$

in which T is the travel time, τ is the origin time, x is the 2D source location, and ∂x is the source location perturbation. The SPDD is then calculated by subtracting equation (4) from (3):

$$\begin{aligned} r_i - r_j &= \sum_{m=1}^2 \left(\frac{\partial T_i}{\partial x_m} - \frac{\partial T_j}{\partial x_m} \right) \Delta x_m \\ &= (T_i - T_j)^{\text{obs}} - (T_i - T_j)^{\text{cal}}, \end{aligned} \quad (5)$$

in which $(T_i - T_j)^{\text{obs}}$ is the observed differential arrival time determined for each station pair through cross correlation of the envelopes, and $(T_i - T_j)^{\text{cal}}$ is the calculated differential travel time. Equation (5) is a linearization of a nonlinear inverse problem, which is solved by iteratively applying the relation in equation (5) and generating new estimates of the calculated differential travel times until convergence with the observed differential travel times is achieved based on root mean square (rms) error. Prior to SPDD location, the detection of an event is performed on a network of stations. First, we set a minimum envelope correlation coefficient threshold of 0.55 for a single station-pair estimate. All station-pair estimates are then analyzed. A detection is made when at least three stations are involved in station-pair estimates in which the envelope correlation coefficient threshold is exceeded. For the 2007 Pavlof data shown in later sections, we require all five working stations, rather than the minimum number of three, be used for detection. This helps achieve higher-quality locations. After detection, locations are accepted if the rms error is less than 1 s. Envelopes are also smoothed using a 1 s convolutional filter.

Results

Out-of-Network Detection and Localization

Following the work of [De Angelis et al. \(2012\)](#), we analyze the GCA from an explosive eruption of Cleveland Volcano in May 2013. We apply STA/LTA analysis of the filtered data and compare it to STA/LTA for the smoothed envelopes and modified spectrogram envelopes. Figure 3b shows a 2–10 Hz filtered record section for the five operating stations on Okmok Volcano, sorted by distance from Cleveland Volcano, with amplitudes normalized. There is a clear arrival on all five stations, typically lasting ~ 30 s. Figure 3b,c shows the same record section, but this time for the smoothed waveform envelopes and modified spectrogram envelopes. STA/LTA analysis of these data corresponding to a propagation velocity across the network of 340 ± 30 m/s from the direction of Cleveland Volcano (240.5°) reveals a clear peak that is visible on all five stations. This corresponds to an acoustic wave from an explosive eruption at Cleveland Volcano at $\sim 12:59$ UTC on 4 May 2013. In fact, automated STA/LTA analysis of the filtered data was used by AVO to detect this explosion in near-real time (similar to [De Angelis et al., 2012](#)). Although clear peaks occur in all iterations of the waveforms, envelopes, and STA/LTA

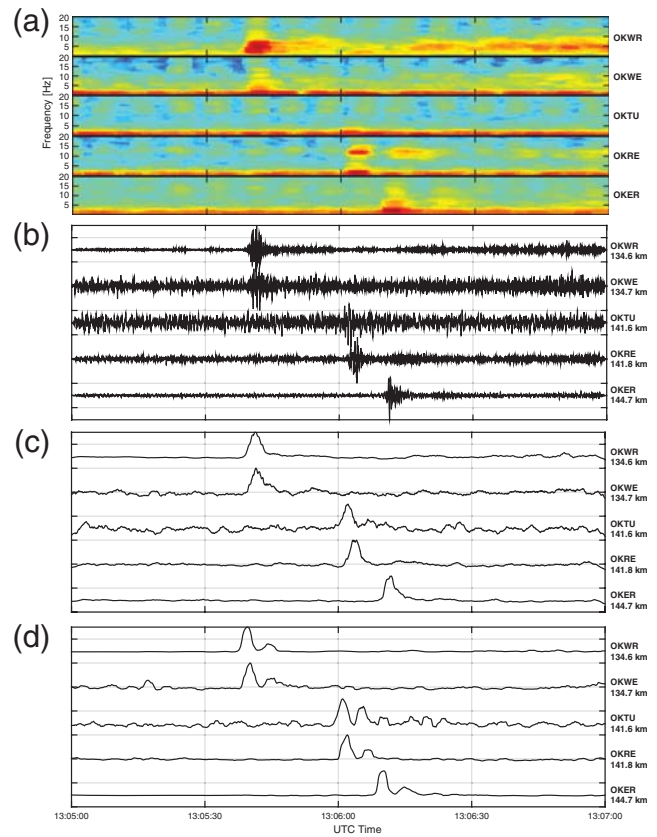


Figure 3. Data from the 5 May 2013 Cleveland Volcano explosion on the Okmok seismic network. (a) Multitaper spectrogram, (b) 2–10 Hz filtered waveforms, (c) smoothed envelopes, and (d) spectrogram envelopes. Amplitudes for each trace are normalized and plotted as a function of distance from the source.

application, the smoothed envelopes and modified spectrograms have the highest overall STA/LTA ratios: peaks of 8–13 and 8–12, respectively, versus 3–14 for the filtered data. This is consistent with analysis of other GCA events from Cleveland Volcano. In addition, the aforementioned STA/LTA methods are focused on impulsive arrivals. Detection of more emergent and long-lasting events, such as volcanic tremor, would likely require modifications to our methods.

The f - k beamforming of the data provides accurate trace velocity and azimuth estimates for the two envelope-based methods but not for the filtered data. Figure 4a–c shows the f - k beamforming results for the 2–10 Hz filtered waveforms, smoothed envelopes, and modified spectrogram envelopes. These plots represent relative beam strength as a function of slowness. We select this frequency band to maximize the SNR. The f - k beamforming for the filtered waveforms reveals two very broad lobes and no clear peak location, whereas the smoothed envelope and modified spectrograms provide realistic estimates of acoustic trace velocity and back azimuth (0.352 km/s, 239.5° and 0.340 km/s, 239.0° , respectively). The beam pattern for the smoothed envelopes is relatively sharp with a single lobe, whereas the beam pattern for the modified spectrogram envelope is slightly broader with a small sidelobe. The actual back

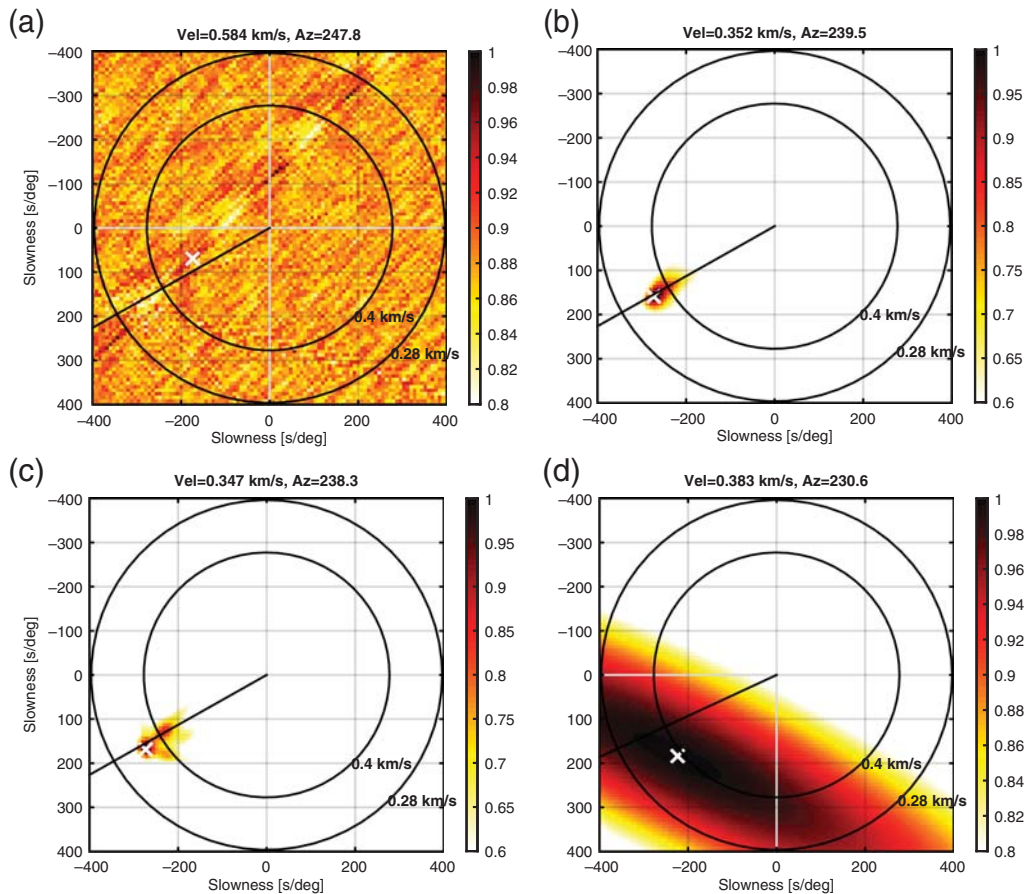


Figure 4. f - k beamforming comparison for the traces in Figure 3. (a) Filtered waveforms, (b) smoothed envelopes, (c) modified spectrogram envelopes, and (d) Okmok infrasound array. The white “x” indicates peak beam power, and the black line indicates the theoretical azimuth to Cleveland. Beamforming for both envelope methods (b,c) provides robust array parameters, in contrast to the marginal results for the filtered waveforms (a) and impaired Okmok infrasound array (d). The beamwidth and sidelobes are smallest for the smoothed envelopes (b).

azimuth to Cleveland Volcano is 240.5° ; and, although the exact trace velocity is unconstrained without accurate temperature data, both estimates are likely close to the actual wave propagation velocity. As expected, cross-correlation values between station pairs are low for the filtered waveforms (~ 0.1 – 0.2) and higher for the smoothed envelopes (0.7 – 0.95) and modified spectrogram envelopes (0.45 – 0.94). Least-squares array processing of the same data produces similar results to the f - k analysis.

This explosion was also recorded by the Okmok infrasound array. At the time of the explosion, only 3/4 of the infrasound array elements were functioning. The three remaining elements form an array roughly perpendicular to a plane wave originating from Cleveland Volcano, which means wave characterization will be poor for the array. The f - k and least-squares analysis of the Okmok infrasound array gives a trace velocity of 0.383 km/s and 230.6° (Fig. 4d), compared to the actual back azimuth of 245.0° and assumed trace velocity of ~ 0.34 km/s. The beam pattern in Figure 4d shows a broad region of beam power and poorly defined maximum. This is likely related to the aforementioned array configuration and missing element. Also of note is that this explosion was recorded as

a GCA on other seismic stations hundreds of kilometers west of Cleveland Volcano, as well as the infrasound array in Dillingham, 992 km to the east.

In-Network Detection and Localization

In-network detection and localization is performed on data from eruptions of Veniaminof and Pavlof Volcanoes. For Veniaminof, we select a three-hour period of seismic data from 11 October 2013. All eight stations of the Veniaminof seismic network were operating at the time, and reports of audible explosions were made from a remote location ~ 60 km northeast of the active vent. We applied the SPDD method to the Veniaminof data and found 25 GCA events coherent on three of eight stations: VNNF, VNHG, and VNSG. The three stations with coherent GCA range between ~ 10 and 21 km from the vent and are located to the east-northeast. Figure 5 shows a 2 min record section filtered between 2 and 10 Hz for these three stations and a map of the station and detection locations. Detection locations cluster within ~ 1 km south of the active vent. The *srcLoc* technique was not able to locate any GCA from Veniaminof Volcano, because it requires a minimum of four stations to function.

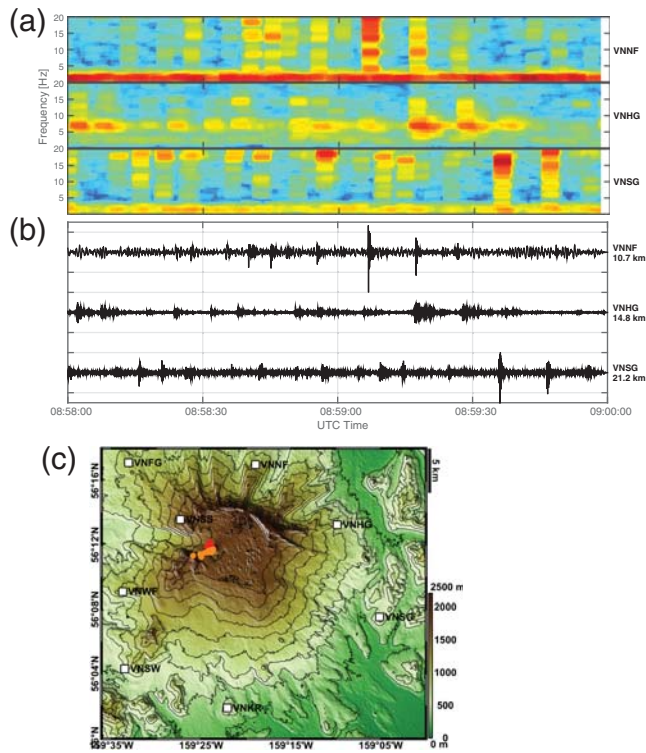


Figure 5. Mt. Veniaminof data and map. (a) Multitaper spectrogram and (b) filtered waveforms for the three stations that detected the ground-coupled airwaves. (c) The topographic map of Veniaminof with the station-pair double difference (SPDD) locations (orange dots). The active vent is denoted by a red triangle and the seismic stations as white squares.

Detection and localization methods are applied to the 2007 and 2013 eruptions of Pavlof Volcano. First, we apply STA/LTA to an explosion from the 2013 eruption. We select an event from 23 May 2013 21:08–21:10 UTC, the same as in Figure 6 of Waythomas *et al.* (2014), in which they used STA/LTA of the envelopes to detect explosions from the eruption. The Pavlof Volcano GCA have relatively high-frequency content, so we filter the data between 7 and 20 Hz (compared to 2–10 Hz for the Okmok data for Cleveland and Veniaminof Volcanoes) and remove the travel time across the network. Figure 6 shows a comparison of the STA/LTA results for the filtered waveforms, smoothed envelope, and modified spectrogram envelopes. Clear peaks are visible for all methods and all stations but are substantially higher for the envelope methods. STA/LTA peaks for filtered waveforms are 2.5–6.5 compared to 9.0–16.0 for the smoothed envelope, and 10.5–24.5 for the modified spectrogram.

SPDD and *srcLoc* are now applied to the 2007 eruption of Pavlof Volcano. Five out of six seismic stations were running at the time (Fig. 1d). Data between 15 August and 15 September 2007 are analyzed for coherent GCA. We first analyze a single explosion for comparison between the methods. Figure 7 shows a record section of the 7–20 Hz filtered waveforms, smoothed envelopes, and SPDD (blue) and *srcLoc* (green) locations. Clear arrivals are apparent on all five stations lasting 5–10 s. A seismic arrival, generally concentrated at lower frequencies (Garces and Hansen, 1998), shows up clearly on the closest stations (PV6 and PN7A). Both methods place the source location for this event roughly 100–200 m east of Pavlof Volcano’s summit (Fig. 7c). Applying SPDD to the rest

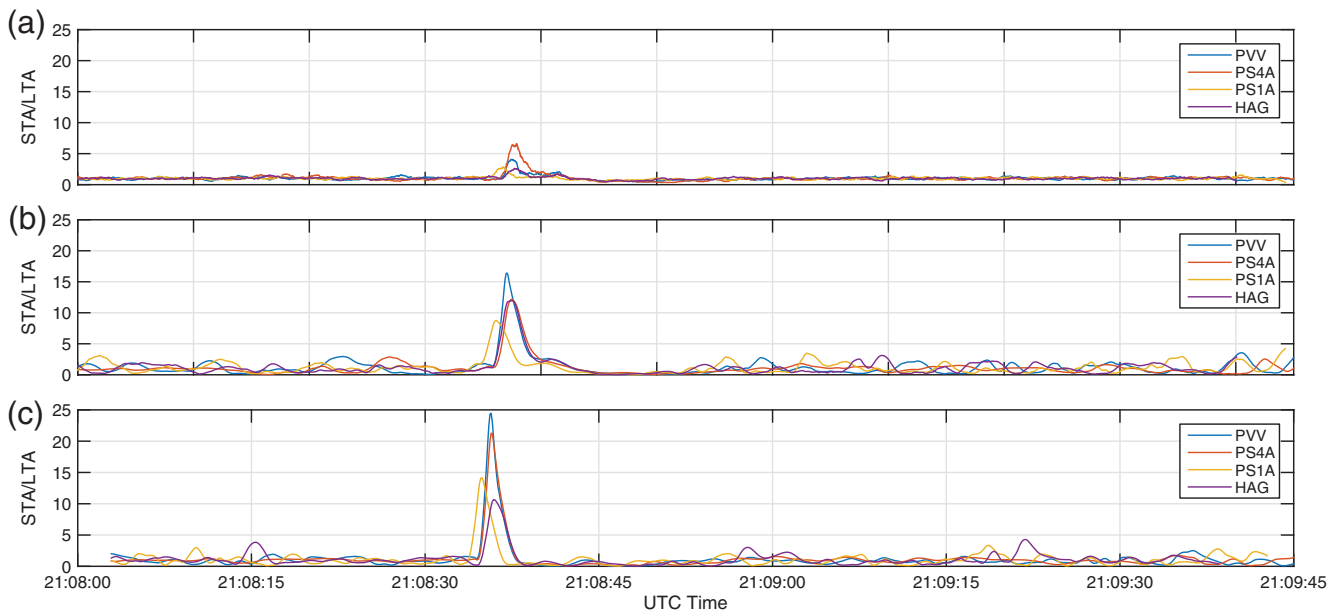


Figure 6. STA/LTA comparison for an explosion from the 2013 Pavlof eruption. STA/LTA ratios for (a) 7–20 Hz filtered waveforms, (b) smoothed envelopes, and (c) modified spectrogram envelopes. Both envelope-based methods produce higher STA/LTA peaks for the explosion.

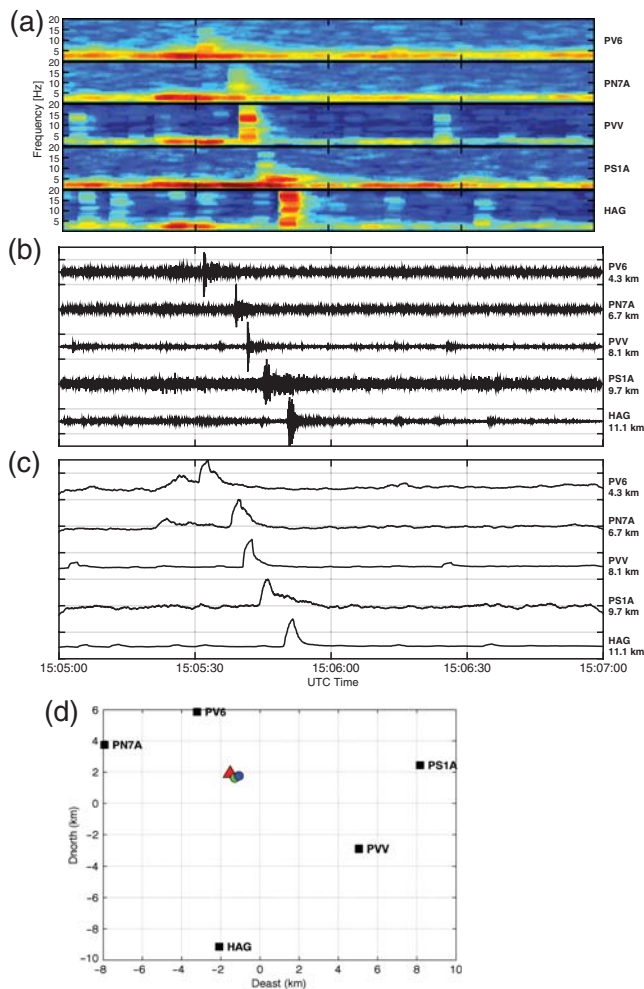


Figure 7. Pavlof Volcano explosion from 2007 with (a) spectrogram, (b) filtered waveforms, (c) smoothed envelopes, and (d) time difference of arrival localization comparison. Both *srcLoc* (green) and SPDD (blue) produce similar locations, 0.38 and 0.46 km, respectively, close to the actual volcanic vent (red).

of the data produces 559 events. These events are plotted in Figure 8 and form a relatively tight cluster east-southeast of the summit, suggesting they are volcanic in origin and that our processing parameters are robust. Application of *srcLoc* to the entire dataset produces similar results.

Discussion

Application of various detection and localization techniques to GCA on volcano-seismic networks in Alaska provides insight into volcanic activity that otherwise is not available using traditional processing. For Cleveland Volcano, as first shown by De Angelis *et al.* (2012), GCA from even moderately sized, impulsive volcanic explosions can be detected on distant seismic networks using relatively standard array processing techniques. This is valuable for detecting volcanic activity in remote areas, such as the Aleutian Islands, that would otherwise go undetected; distinguishing between seismic and acoustic events on a seismic network; and differ-

entiating nonvolcanic versus volcanic events. Our results suggest event detection, timing, and back-azimuth and trace-velocity estimates appear robust and compare favorably to theoretical values. This is particularly true when the waveform envelopes are smoothed and modified using a spectrogram-derived envelope. The GCA results are also more accurate compared to those from a nearby infrasound array. This infrasound array had a sub-optimal array response due to a nonfunctional element, which contributed to its poor wave-parameter estimation. We believe a fully operational infrasound array would provide similar results to the GCA processing. Note that amplitude information is not obtained using these techniques, so the explosion strength is unconstrained.

The TDOA methods provided robust localization of GCA events as well. For the Veniaminof eruption, near-constant seismic tremor was detected over a period of many months (Schneider *et al.*, 2013), but differentiating subsurface tremor versus surface degassing and explosions was difficult. Application of the SPDD technique to the seismic network for a three-hour test period revealed coherent acoustic waves that are interpreted as explosions from the active vent. These explosions were not detected with other methods at this difficult-to-monitor volcano. Eruption style and potential hazard are thus better understood and characterized. For Pavlof Volcano, GCA have been studied in the past to examine the volcanic conduit and number of explosions (Garces and Hansen, 1998; Waythomas *et al.*, 2014). Similar to Veniaminof Volcano, our methods permit the detection of acoustic waves (hence explosions) and distinguishing between subsurface (seismic) and surface (acoustic) activity. This has important implications for hazard monitoring for Pavlof Volcano, as explosive degassing and subsequent acoustic waves suggest the potential for hazardous ash plumes (Fee and Matoza, 2013). Pavlof Volcano often transitions from sustained lava fountaining to short-duration, repeating explosions (Waythomas *et al.*, 2014), and the methods presented here permit a distinction between the two.

STA/LTA ratios are commonly used for detection of events. The smoothed and modified spectrogram envelopes shown here produce higher STA/LTA ratios than filtered waveforms alone. GCA events are often difficult to detect due to low SNR, and therefore these methods are valuable for increased event detection. It is likely that these methods could improve STA/LTA ratios of other seismic events.

Pavlof Volcano often erupts at different locations on the summit, and the vent location has important hazard implications (Waythomas *et al.*, 2014). In 2007, the primary eruptive vent was ~ 130 m southeast of the summit (Fig. 8c), which is consistent with the clustering of GCA in Figure 8a,b. This suggests TDOA methods may provide relatively high-resolution (< 200 m) localization of GCA using typical volcano seismic networks (e.g., 5+ seismic stations over an $\sim 15 \times 15$ km² region). It may also be possible to differentiate between multiple vents and track the opening of new fissures (e.g., Cannata *et al.*, 2011; Fee *et al.*, 2011).

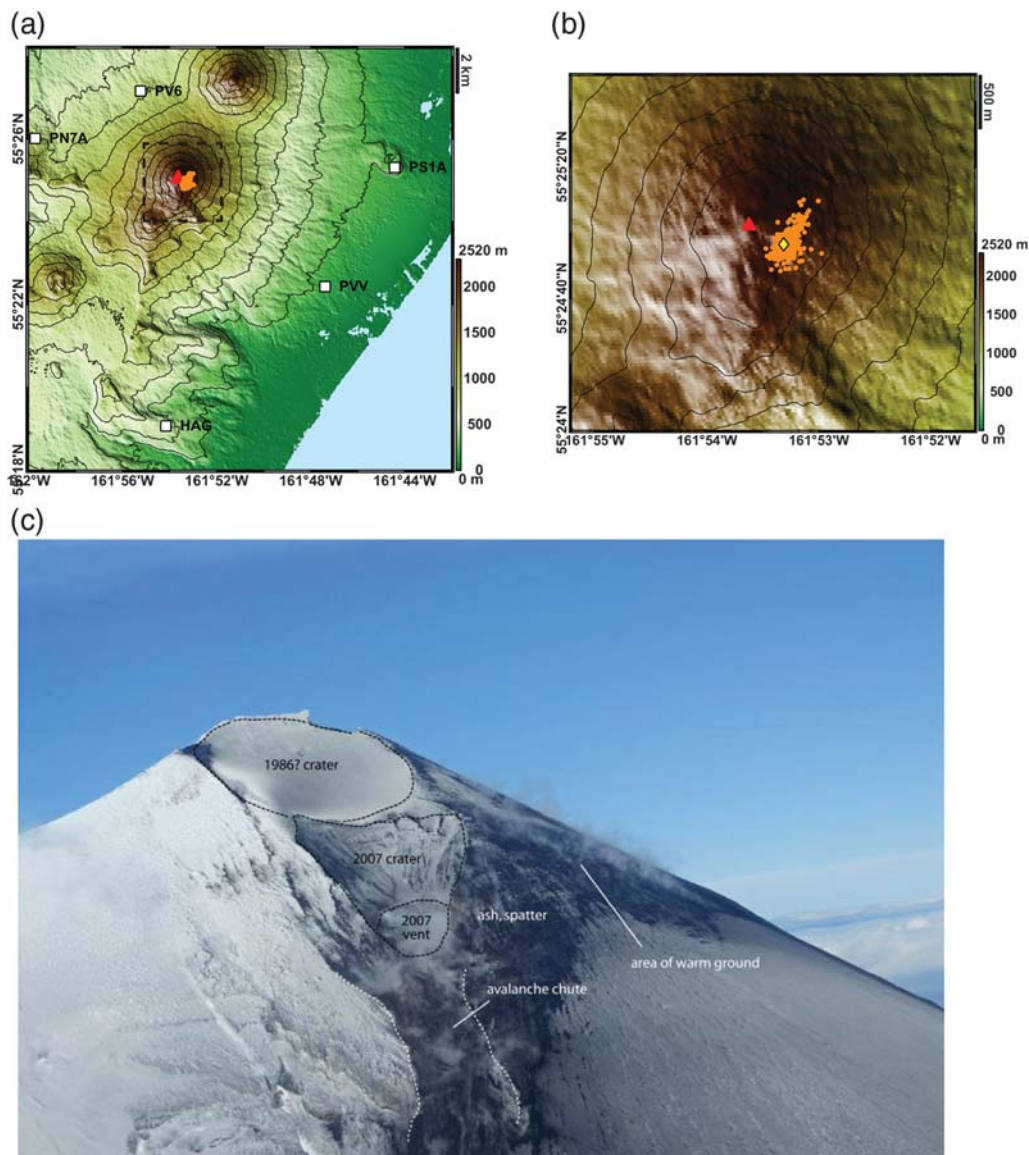


Figure 8. SPDD locations for the 2007 Pavlof eruption. (a) Topographic map of the Pavlof seismic network (white squares), summit (red triangle), and SPDD locations (orange dots). (b) Enlarged view of the Pavlof summit. Yellow diamond denotes actual vent location, which is in good agreement with the SPDD locations. (c) Photograph of the south flank of Pavlof Volcano, showing the summit and actual vent location. (Photo by C. Waythomas, Alaska Volcano Observatory [AVO]).

We now comment on the resolution of our TDOA localization methods at Pavlof Volcano using synthetic data and forward modeling. Similar to Rowell *et al.* (2014), we create synthetic signals with varying SNR originating from Pavlof Volcano's summit and propagating out to each station at 340 m/s. Our synthetic data for each channel consists of a 10 s broadband signal inserted into a 120 s data segment. Both the signal and noise have a $1/f$ rolloff and are generated using random numbers. We then vary the SNR at 0, 0.5, 1, and 5 dB. The data are filtered, and the smoothed envelope is taken and inserted into both *srcLoc* and SPDD. Figure 9 shows the synthetic location results for both methods with 1000 iterations for each SNR value, along with 95% confi-

dence intervals. The *srcLoc* confidence intervals for each SNR are as follows: SNR = 0, $\sim 340 \times 700$ m; SNR = 0.5, $\sim 290 \times 560$ m; SNR = 1, $\sim 240 \times 500$ m; and SNR = 5, $\sim 80 \times 170$ m. The SPDD confidence intervals are similar in size: SNR = 0, $\sim 400 \times 430$ m; SNR = 0.5, $\sim 430 \times 470$ m; SNR = 1, $\sim 280 \times 310$ m; and SNR = 5, $\sim 60 \times 70$ m. Explosion GCAs at Pavlof Volcano generally have SNRs > 1 dB and often > 5 dB, so *srcLoc* and SPDD have the potential to locate sources within ~ 100 m of the true source for the five-station Pavlof network. This further suggests the clustering of events to the southeast of Pavlof Volcano's summit in 2007 is a source feature rather than a resolution issue and indicates promise for future applications. We further note

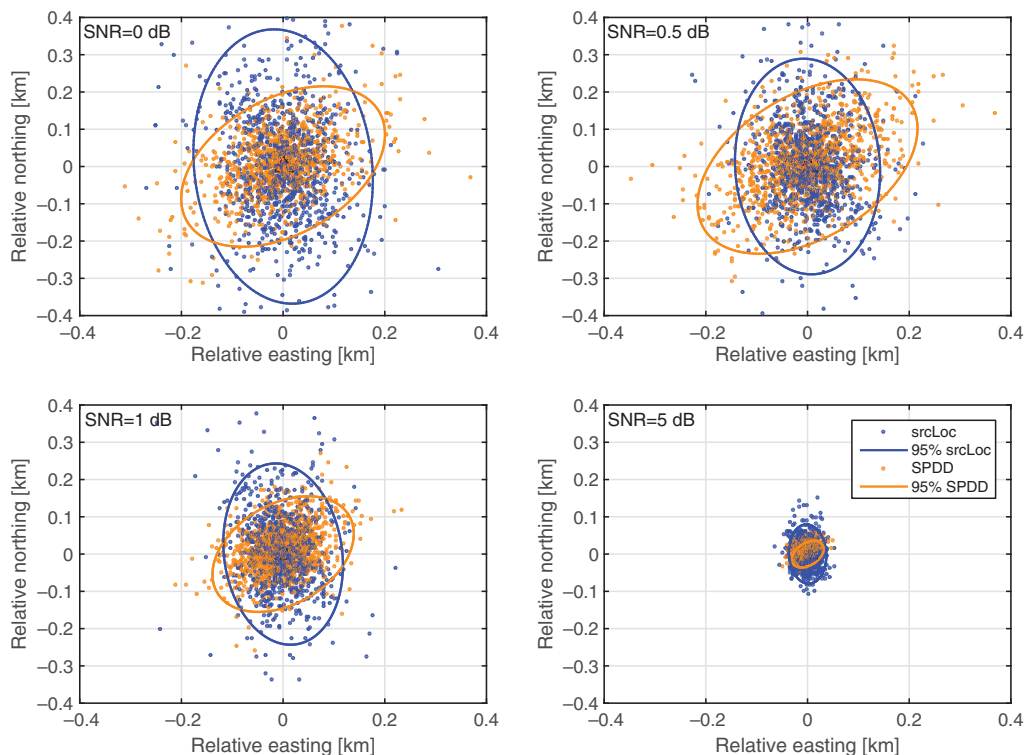


Figure 9. Resolution tests for the Pavlof Volcano seismic network for *srcLoc* (blue) and SPDD (orange). Dots denote locations of synthetic data for various signal-to-noise ratios (SNRs): (a) 0 dB, (b) 0.5 dB, (c) 1 dB, and (d) 5 dB. The ellipses indicate 95% confidence intervals, and the red triangle indicates the source location. Both methods produce similar resolution.

that, although a 1D velocity structure seems reasonable for Pavlof Volcano, we still expect the GCA waveforms between stations to be incoherent (thus necessitating the use of envelopes and incoherent array processing). Green (2015) showed that coherence loss between infrasound sensors can be significant at scale lengths of even a few kilometers, largely due to signal multipathing.

The TDOA methods presented here have assumptions and limitations that may reduce their effectiveness. First, the efficiency of air-ground coupling may be variable and depend on numerous factors such as near-surface geology, frequency, topography, etc. (e.g., Madshus *et al.*, 2005; Hinzen, 2007). Our methods assume a constant sound velocity, thus advection of sound from wind, scattering from topography, and differences between source-receiver elevations may all cause significant deviations in the actual travel times (Fee and Matoza, 2013). For the Pavlof data, a constant velocity seems reasonable, because the localization is fairly tightly clustered and close to the actual source. The Veniaminof GCA were only detected to the east-northeast, which is consistent with regional winds blowing strongly to the northeast, and perhaps variable coupling. Upwind propagation to the other stations is likely hindered. This may partially explain the relatively large offset (> 1 km) in the source location as well. Our methods also assume a single point source. Extended sources and multiple sources are better suited for backprojection techniques (Walker

and Shearer, 2009; Haney, 2014). The smoothing of the envelope likely reduces the resolution of the source location as well, although it provides a general increase in coherence. The variety of seismic networks in the world and variable source-receiver ranges requires multiple techniques be used (e.g., planar versus spherical waves propagating across the network). Finally our method is tuned primarily to impulsive signals (explosions), rather than sustained signals (tremor or jetting). (See Fee and Matoza, 2013, and Matoza *et al.*, 2014, for a more in-depth discussion of volcano infrasound signal properties.)

Conclusions

Multiple methods are explored for detection and localization of GCA on volcano-seismic networks in Alaska. We use envelope-based techniques, because the GCA waveforms are typically not coherent between stations separated by kilometers. These detection and location techniques are effective for GCA on a variety of networks. STA/LTA-based detection is improved by using smoothed envelopes and modified envelopes derived from spectrograms that emphasize time periods with both high energy and high-energy contrast. Back azimuth and trace velocity for GCA are accurately determined for an explosion from Cleveland Volcano on a distant seismic network. These parameters are more accurate than the parameters estimated using data from a nearby infrasound array hindered by a missing element, supporting the

use of GCA in this situation. Two different TDOA methods are used for a spherical acoustic wave propagating across a seismic network. Both methods produced fairly high-resolution localization of volcanic sources at Veniaminof and Pavlof Volcanoes. The five-station Pavlof seismic network is able to locate acoustic events to within ~ 100 m of the actual source, which, for the 2007 eruption, corresponds to a vent southeast of the summit.

The methods presented here can provide fairly robust detection, parameter estimation, and location of acoustic sources recorded by seismic networks. GCA can help characterize explosive activity for remote or sparsely monitored volcanoes that are difficult to access, such as those in Alaska. We have now implemented these methods at AVO for Cleveland and Pavlof Volcanoes and are using these techniques for detection of future activity and to distinguish between different types of events. Future improvements for both research and monitoring purposes could involve using a combination of seismic and acoustic networks (to increase station density) and more advanced propagation modeling and localization (Kim and Lees, 2015). These methods could also be helpful in chemical and nuclear explosion monitoring. Finally seismic–acoustic coherence of collocated sensors (Matoza and Fee, 2014) may also help differentiate between signal and noise (as a function of frequency) and improve timing constraints.

Data and Resources

Seismic data used in this article came from the Alaska Volcano Observatory (AVO) network and are available at the Incorporated Research Institutions for Seismology Data Management Center (www.iris.edu, last accessed December 2015). Observations of volcanic activity were made by AVO and are detailed on its website (www.avo.alaska.edu, last accessed December 2015). Topographic maps were created using ASTER and ETOPO5 digital elevation model data.

Acknowledgments

Funding was provided by National Science Foundation Grants EAR-1331084 and EAR-1113338, the Alaska Volcano Observatory, and the University of Alaska Fairbanks Geophysical Institute. Reviews by Jim Dixon and two anonymous reviewers provided helpful comments to improve the paper.

References

- Ben-Menahem, A., and S. J. Singh (1981). *Seismic Waves and Sources*, Springer Science and Business Media, New York, New York.
- Cannata, A., M. Sciotto, L. Spampinato, and L. Spina (2011). Insights into explosive activity at closely-spaced eruptive vents using infrasound signals: Example of Mt. Etna 2008 eruption, *J. Volcanol. Geoth. Res.* **208**, 1–11.
- Cochran, E., and P. Shearer (2006). Infrasound events detected with the southern California seismic network, *Geophys. Res. Lett.* **33**, L19803, 1–5, doi: [10.1029/2006GL026951](https://doi.org/10.1029/2006GL026951).
- De Angelis, S., D. Fee, M. Haney, and D. Schneider (2012). Detecting hidden volcanic explosions from Mt. Cleveland Volcano, Alaska with infrasound and ground-coupled airwaves, *Geophys. Res. Lett.* **39**, L21312, doi: [10.1029/2012gl053635](https://doi.org/10.1029/2012gl053635).
- Dixon, J. P., C. Cameron, R. G. McGimsey, C. A. Neal, and C. Waythomas (2015). 2013 volcanic activity in Alaska: Summary of events and response of the Alaska Volcano Observatory, *U.S. Geol. Surv. Open-File Rept. 2015-5110*, 92 pp.
- Edwards, W. N., D. W. Eaton, P. J. McCausland, D. O. ReVelle, and P. G. Brown (2007). Calibrating infrasonic to seismic coupling using the Stardust sample return capsule shockwave: Implications for seismic observations of meteors, *J. Geophys. Res.* **112**, no. B10306, 1–13, doi: [10.1029/2006JB004621](https://doi.org/10.1029/2006JB004621).
- Fee, D., and R. S. Matoza (2013). An overview of volcano infrasound: From Hawaiian to Plinian, local to global, *J. Volcanol. Geoth. Res.* **249**, 123–139.
- Fee, D., M. Garces, T. R. Orr, and M. P. Poland (2011). Infrasound from the 2007 fissure eruptions of Kilauea Volcano, Hawai'i, *Geophys. Res. Lett.* **38**, L06309, doi: [10.1029/2010GL046422](https://doi.org/10.1029/2010GL046422).
- Garces, M. A., and R. A. Hansen (1998). Waveform analysis of seismoacoustic signals radiated during the fall 1996 eruption of Pavlof Volcano, Alaska, *Geophys. Res. Lett.* **25**, 1051–1054.
- Gibbons, S. J. (2014). The applicability of incoherent array processing to IMS seismic arrays, *Pure Appl. Geophys.* **171**, 377–394.
- Gibbons, S. J., F. Ringdal, and T. Kværna (2008). Detection and characterization of seismic phases using continuous spectral estimation on incoherent and partially coherent arrays, *Geophys. J. Int.* **172**, 405–421.
- Green, D. N. (2015). The spatial coherence structure of infrasonic waves: Analysis of data from International Monitoring System arrays, *Geophys. J. Int.* **201**, 377–389.
- Haney, M. M. (2010). Location and mechanism of very long period tremor during the 2008 eruption of Okmok Volcano from interstation arrival times, *J. Geophys. Res.* **115**, no. B00B05, 1–13, doi: [10.1029/2010JB007440](https://doi.org/10.1029/2010JB007440).
- Haney, M. M. (2014). Backprojection of volcanic tremor, *Geophys. Res. Lett.* **41**, 1923–1928.
- Haney, M. M., K. van Wijk, L. A. Preston, and D. F. Aldridge (2009). Observation and modeling of source effects in coda wave interferometry at Pavlof Volcano, *TLE* **28**, 554–560.
- Hedlin, M. A., C. de Groot-Hedlin, and D. Drob (2012). A study of infrasound propagation using dense seismic network recordings of surface explosions, *Bull. Seismol. Soc. Am.* **102**, 1927–1937.
- Hinzen, K.-G. (2007). London fuel tank explosion recorded by short-period seismic stations at 500-km distance, *Seismol. Res. Lett.* **78**, 383–388.
- Ichihara, M., M. Takeo, A. Yokoo, J. Oikawa, and T. Ohminato (2012). Monitoring volcanic activity using correlation patterns between infrasound and ground motion, *Geophys. Res. Lett.* **39**, L04304, doi: [10.1029/2011GL050542](https://doi.org/10.1029/2011GL050542).
- Johnson, D. H., and D. E. Dudgeon (1992). *Array Signal Processing: Concepts and Techniques*, Simon and Schuster, Englewood Cliffs, New Jersey.
- Johnson, J. B., and S. D. Malone (2007). Ground-coupled acoustic airwaves from Mount St. Helens provides constraints on the May 18th, 1980 eruption, *Earth Planet. Sci. Lett.* **258**, 16–31.
- Kim, K., and J. M. Lees (2015). Imaging volcanic infrasound sources using time reversal mirror algorithm, *Geophys. J. Int.* **202**, 1663–1676.
- Madshus, C., F. Løvholt, A. Kaynia, L. R. Hole, K. Attenborough, and S. Taherzadeh (2005). Air–ground interaction in long range propagation of low frequency sound and vibration: Field tests and model verification, *Appl. Acoust.* **66**, 553–578.
- Matoza, R. S., and D. Fee (2014). Infrasonic component of volcano–seismic eruption tremor, *Geophys. Res. Lett.* **41**, 1964–1970, doi: [10.1002/2014gl059301](https://doi.org/10.1002/2014gl059301).
- Matoza, R. S., D. Fee, and T. M. López (2014). Acoustic characterization of explosion complexity at Sakurajima, Karymsky, and Tungurahua Volcanoes, *Seismol. Res. Lett.* **85**, 1187–1199, doi: [10.1785/0220140110](https://doi.org/10.1785/0220140110).
- Miller, T. P., R. G. McGimsey, D. H. Richter, J. R. Riehl, C. J. Nye, M. E. Yount, and J. A. Dumoulin (1998). Catalog of the historically active volcanoes of Alaska, *U.S. Geol. Surv. Open-File Rept. 98-0582*, 104 pp.
- Obara, K. (2002). Nonvolcanic deep tremor associated with subduction in southwest Japan, *Science* **296**, 1679–1681.

- Rowell, C. R., D. Fee, C. A. L. Szuberla, K. Arnoult, R. S. Matoza, P. P. Firstov, K. Kim, and E. Makhmudov (2014). Three-dimensional volcano-acoustic source localization at Karymsky Volcano, Kamchatka, Russia, *J. Volcanol. Geoth. Res.* **283**, 101–115.
- Schneider, D., C. Waythomas, K. Wallace, M. Haney, D. Fee, M. Pavlonis, and C. Read (2013). The 2013 eruptions of Pavlof and Mount Veniaminov Volcanoes, Alaska, *AGU Fall Meeting Abstracts*, Abstract V23C–2840.
- Szuberla, C. A., and K. M. Arnoult (2011). Locating explosions, volcanoes, and more with infrasound, *Phys. Today* **64**, 74.
- Szuberla, C. A. L., K. M. Arnoult, and J. V. Olson (2006). Discrimination of near-field infrasound sources based on time-difference of arrival information, *J. Acoust. Soc. Am.* **120**, EL23–EL28.
- Szuberla, C. A. L., J. V. Olson, and K. M. Arnoult (2009). Explosion localization via infrasound, *J. Acoust. Soc. Am.* **126**, EL112–EL116.
- Thomson, D. J. (1982). Spectrum estimation and harmonic analysis, *Proc. IEEE* **70**, 1055–1096.
- Waldhauser, F., and W. L. Ellsworth (2000). A double-difference earthquake location algorithm: Method and application to the northern Hayward fault, California, *Bull. Seismol. Soc. Am.* **90**, 1353–1368.
- Walker, K. T., and P. M. Shearer (2009). Illuminating the near-sonic rupture velocities of the intracontinental Kokoxili M_w 7.8 and Denali fault M_w 7.9 strike-slip earthquakes with global P wave back projection imaging, *J. Geophys. Res.* **114**, no. B02304, 1–21, doi: [10.1029/2008JB005738](https://doi.org/10.1029/2008JB005738).
- Walker, K. T., R. Shelby, M. A. Hedlin, C. Groot-Hedlin, and F. Vernon (2011). Western US Infrasonic Catalog: Illuminating infrasonic hot spots with the USArray, *J. Geophys. Res.* **116**, no. B12305, 1–15, doi: [10.1029/2011JB008579](https://doi.org/10.1029/2011JB008579).
- Waythomas, C. F., M. M. Haney, D. Fee, D. J. Schneider, and A. Wech (2014). The 2013 eruption of Pavlof Volcano, Alaska: A spatter eruption at an ice- and snow-clad volcano, *Bull. Volcanol.* **76**, 1–12.
- Waythomas, C. F., S. G. Prejean, and S. R. McNutt (2008). Alaska's Pavlof Volcano ends 11-year repose, *Eos Trans. AGU* **89**, 209–211.
- Withers, M., R. Aster, C. Young, J. Beiriger, M. Harris, S. Moore, and J. Trujillo (1998). A comparison of select trigger algorithms for automated global seismic phase and event detection, *Bull. Seismol. Soc. Am.* **88**, 95–106.
- Zhang, H., R. M. Nadeau, and M. N. Toksoz (2010). Locating nonvolcanic tremors beneath the San Andreas fault using a station-pair double-difference location method, *Geophys. Res. Lett.* **37**, L13304, 1–6, doi: [10.1029/2010GL043577](https://doi.org/10.1029/2010GL043577).

Alaska Volcano Observatory
Geophysical Institute
University of Alaska Fairbanks
903 Koyukuk Drive, Room 506G
Fairbanks, Alaska 99775
dfee1@alaska.edu
(D.F.)

Alaska Volcano Observatory
U.S. Geological Survey
4230 University Drive
Anchorage, Alaska 99508
(M.H., J.L., C.W.)

Department of Earth Science and Earth Research Institute
University of California, Santa Barbara
1006 Webb Hall
Santa Barbara, California 93106
(R.M.)

Wilson Alaska Technical Center
Geophysical Institute
University of Alaska Fairbanks
903 Koyukuk Drive
Fairbanks, Alaska 99775
(C.S.)

Manuscript received 22 February 2016;
Published Online 5 April 2016